Sensitivity analysis and passive control of the secondary instability in the cylinder wake

By F. GIANNETTI[1], S. CAMARRI[2], V. CITRO[1]

1 DIIN, Universitá di Salerno, 84084 Fisciano (SA), Italy

2 Dipartimento di Ingegneria Aerospaziale, Università di Pisa, Italy

(Received August 27, 2018)

The stability properties of selected flow configurations, usually denoted as base flows, can be significantly altered by small modifications of the flow, which can be caused for instance by a non-intrusive passive control. This aspect is amply demonstrated in the literature by ad-hoc sensitivity studies which, however, focus on configurations characterised by a steady base flow. Nevertheless, several flow configurations of interest are characterised by a time-periodic base flow. To this purpose, we propose here an original theoretical framework apt to quantify the effects of base-flow variations in the stability properties of saturated time-periodic limit cycles. In particular, starting from a Floquet analysis of the linearised Navier-Stokes equations and using adjoint methods it is possible to estimate the variation of a selected Floquet exponent caused by a generic structural perturbation of the base-flow equations. This link is expressed concisely using the adjoint operators coming from the analysis and the final result, when applied to spatially localised disturbances, is used to build spatial sensitivity and control maps. These maps identify the regions of the flow where the placement of a infinitesimal small object produces the largest effect on the Floquet exponent and may also provide a quantification of this effect. Such analysis brings useful insights both for passive control strategies and further characterise the investigated instability. As an example of application, the proposed analysis is applied here to the three-dimensional flow instabilities in the wake past a circular cylinder. This is a classical problem which has been widely studied in the literature. Nevertheless, by applying the proposed analysis we derive original results comprising a further characterisation of the instability and control maps. We finally show that the control maps obtained here are in very good agreement with control experiments documented in the literature.

1. Introduction

Stability and sensitivity analysis of a flow configuration (base flow) is important both for investigating the path followed by the flow to depart from the selected configuration when this is unstable and for the identification of possible controls of an identified instability. Passive controls generally lead to ad-hoc modifications of the base flow which change its stability properties in a desired way. In particular, the dynamics of small disturbances superposed to the reference state is modified by a passive control in two ways: (i) by a modification of the base flow and (ii) by a direct action of the control on the dynamics itself. This aspect is well illustrated for instance in Luchini *et al.* (2009) and Marquet *et al.* (2008) where stability and sensitivity analysis is applied so as to investigate the passive control of the vortex shedding instability in the wake past a circular cylinder excerted by using a small control rod positioned in the wake. In the referenced

paper it is shown that the two contributions of the control, i.e. the modification of the base flow and its direct action on the disturbance dynamics, both play an important role in the modification of the instability. Moreover, a strategy is proposed so as to derive control maps predicting the effect of the control rod for a generic position of its center using adjoint methods. The same idea and methods have been successively applied in the literature to a wide variety of flow instabilities (see for instance the review in Camarri (2015)).

A key ingredient in the method proposed in Marquet *et al.* (2008) is the sensitivity analysis of a selected global instability to a variation of the base flow which can be induced by a generic forcing of the momentum equations. This aspect alone, even without the implications it may have for control purposes, plays a significant role in the characterisation of the instability, as also underlined in Sipp *et al.* (2010); Luchini & Bottaro (2014); Camarri (2015).

The first sensitivity analysis to a base flow modification is documented in Bottaro *et al.* (2003), where the authors assessed the sensitivity of the Orr-Sommerfeld spectrum to a generic modification of the base flow for the plane Couette flow. They used variational techniques to determine the mean-flow modification of prescribed magnitude having the largest effect on a selected eigenmode. Small base flow variations were found to be sufficient to destabilize the flow that is otherwise unconditionally stable according to linear stability analysis, this last aspect being in contrast to experimental evidence. Gavarini *et al.* (2004) studied the effect of base-flow distortions in the transition process of cylindrical pipe flows. The sensitivity of the singular values of the resolvent operator of the linearised flow dynamics with respect to base-flow modifications was studied by Brandt *et al.* (2011) who derived the analytical expression for the gradient of the resolvent norm of the system with respect to the base-flow modifications.

All the studies documented in the literature on sensitivity analysis to base-flow perturbations, and in particular all the references cited above, consider steady base flows. However, sensitivity analysis to base-flow modifications is also relevant for configurations in which the base flow is periodic in time. Several important flow instabilities can be included in this case, as for instance the secondary instability occurring in plane wakes past bluff-bodies leading the flow from a two- to a three-dimensional state. A partial result in this respect is documented in Giannetti *et al.* (2010) where the sensitivity of the three-dimensional secondary instability of a circular-cylinder wake to a structural perturbation of the linearized Navier-Stokes equations is investigated by adjoint methods. To this purpose, the work in Giannetti *et al.* (2010) generalizes the approach originally proposed by Giannetti & Luchini (2007) to investigate the first instability of the cylinder wake so as to include the case of time-periodic baseflows. In particular, the authors identify a localised region of maximum coupling among the velocity components by using the direct and adjoint Floquet mode associated to the selected 3D instability. The resulting sensitivity field takes into account the feedback which is at the origin of the self-excited oscillation and is therefore useful to locate the region where the instability mechanism acts. The theoretical approach proposed in Giannetti *et al.* (2010) investigates only one among the two ways in which the dynamics of small perturbations on a time-periodic base flow can be affected by a passive control, i.e. by a direct action of a control on the disturbance dynamics. Conversely, the indirect effect of a base flow modification on the dynamics of small disturbances is unexplored and this is the main objective of the present work.

In this paper we propose a framework, based on adjoint methods, which allows to quantify the variation of a given Floquet multiplier caused by a generic variation of the

time-periodic base flow which can be obtained by a generic localised forcing applied to the flow equations.

In this respect the theory proposed here, integrated with the work in Giannetti *et al.* (2010), can be considered as a generalisation of the work by Marquet *et al.* (2008) capable to include base flows which are periodic in time. The main original contribution of this paper is the quantification of the effects that a generic perturbation of the momentum equations can induce on an identified instability. This result alone provides an original and important characterisation of the considered instability, as already discussed. Moreover, when coupled with the theory proposed in Giannetti *et al.* (2010), it provides a framework to design passive controls for instabilities developing on a time-periodic base flow.

As an example of application of the proposed theory we consider the well-known 3D instability of the wake past a circular cylinder, which is an important paradigmatic instability and, for this reason, is widely investigated in the literature. Concisely, Noack *et al.* (1993) and Noak & Eckelmann (1994) found that the flow past a circular cylinder is unstable to three-dimensional perturbations when the flow Reynolds number exceeds a given treshold. Successively, accurate numerical simulations carried out by Barkley & Henderson (1996) confirmed the existence of two separate bands of synchronous unstable modes: mode A ($Re^A_{cr} = 189$) which is characterized by a spanwise wavelength of about 4 cylinder diameters, and mode B ($Re^B_{cr} = 259$) that has a spanwise wavelength of about one diameter. Direct numerical simulations and experimental investigations confirm the existence of these instabilities (Williamson 1988). In such context, the sensitivity analysis carried out here, besides being an example of application of the proposed theory, also provides new and important information pertaining the nature and the control of the secondary instability in the wake past a circular cylinder. Moreover, control maps are derived and validated, and they are shown to be in excellent agreement with the experiments documented in Zhang *et al.* (1995).

Despite of the particular application detailed here, the formulation proposed is general and can be used without any conceptual difficulty to analyze generic base flows that are periodic in time.

After having introduced the problem of the secondary instability in the wake past a circular cylinder and concisely recalled the Floquet stability analysis in section 2, we present the original method proposed here in section 3. In section 4 we merge the results obtained here with those in Giannetti *et al.* (2010) and, as a result, we provide the tools for estimating the effect of a local velocity-force feedback, which may mimick for instance the effect of a control wire as used in Zhang *et al.* (1995), on the secondary instability. Using the numerical methods described in section 5 we show the original results obtained for the cylinder wake in sections 6.

2. Flow configuration and Floquet analysis

In this section, after having introduced the considered flow configuration, we concisely describe the tools for investigating the stability analysis of a time-periodic base flow by a Floquet analysis.

2.1. *Flow configuration*

The incompressible flow around a nominally two-dimensional circular cylinder is considered here and the theory is presented focusing on this specific case, as discussed in the introduction. The flow is described using a Cartesian coordinate system with the z-axis coinciding with the cylinder axis and with the x-axis aligned with the direction of the incoming uniform flow. The flow is governed by the unsteady incompressible Navier-Stokes

equations, which are made dimensionless using the cylinder diameter D^* as the characteristic length scale, the velocity of the incoming stream U^*_∞ as the reference velocity and the (constant) fluid density ρ^*:

$$\frac{\partial \mathbf{U}}{\partial t} + \mathbf{U}\cdot\nabla\mathbf{U} = -\nabla P + \frac{1}{Re}\boldsymbol{\Delta}\mathbf{U} \tag{2.1a}$$

$$\nabla\cdot\mathbf{U} = 0 \tag{2.1b}$$

where $\mathbf{U}$ is the normalised velocity vector with components $\mathbf{U} = (U, V, W)$, P is the reduced pressure and $Re = U^*_\infty D^*/\nu^*$ is the Reynolds number (ν^* being the kinematic viscosity of the fluid). As for the boundary conditions of the continuous problem, no-slip and no-penetration conditions are applied on the cylinder surface Γ_c and the flow is assumed to asymptotically approach the incoming uniform stream in the far field.

2.2. *Floquet analysis*

The considered flow becomes periodic in time when the Reynolds number exceeds a critical value $Re_{c1} \approx 47$, as widely investigated in the literature (see for instance Giannetti & Luchini (2007)). The three-dimensional instability occurring in the resulting time-periodic wake can be investigated using Floquet theory (see, for instance, Drazin (2002)), which is now concisely described.

The Floquet analysis is carried out in order to investigate the stability properties of a time-periodic solution of equation (2.1), $\mathbf{Q_b} = (\mathbf{U}_b, P_b)$ of period T. In the specific case of the considered wake, $\mathbf{Q_b}$ is also a plane two-dimensional flow in the $x-y$ plane. Thus we have $\mathbf{Q_b}(x, y, t+T) = \mathbf{Q_b}(x, y, t)$ and $\mathbf{U}_b \cdot \mathbf{e}_z = 0$, $\mathbf{e}_z$ begin the versor of the z direction. It is assumed that a generic unsteady and three-dimensional perturbation is superposed to the base flow $\mathbf{Q_b}$ thus leading to the total flow field $\mathbf{Q} = \{\mathbf{U}, P\}$:

$$\mathbf{U}(x, y, z, t) = \mathbf{U}_b(x, y, t) + \epsilon \, \frac{1}{\sqrt{2\pi}} \int_{-\infty}^{\infty} \mathbf{u}(x, y, k, t) \;\; \exp(\mathrm{i}kz)\mathrm{d}k \tag{2.2a}$$

$$P(x, y, z, t) = P_b(x, y, t) + \epsilon \, \frac{1}{\sqrt{2\pi}} \int_{-\infty}^{\infty} p(x, y, k, t) \;\; \exp(\mathrm{i}kz)\mathrm{d}k \tag{2.2b}$$

where ϵ is the disturbance amplitude and $\mathbf{u}$ and p are the velocity and pressure disturbances Fourier-transformed in the spanwise direction (an homogeneous direction for the base flow). Introducing (2.2) in (2.1) and linearising in ϵ, we obtain two problems describing respectively the evolution of the 2D periodic base flow and the dynamics of the 3D perturbations. In particular, the base flow is governed by the 2D version of (2.1), while the perturbation field is described by the three-dimensional unsteady linearised Navier-Stokes equations (LNSE). When the Fourier transform in the z direction is applied to the LNSE, for each wavenumber k the following set of equations is obtained:

$$\frac{\partial \mathbf{u}}{\partial t} + \mathcal{L}_k\{\mathbf{U}_b, Re\}\mathbf{u} + \nabla_k p = \mathbf{0} \tag{2.3a}$$

$$\nabla_k \cdot \mathbf{u} = 0 \tag{2.3b}$$

where $\nabla_k \equiv (\frac{\partial}{\partial x}, \frac{\partial}{\partial y}, \mathrm{i}k)$ is the Fourier-transformed gradient operator, $\mathcal{L}_k$ stands for the Fourier-transformed linearised Navier-Stokes operator:

$$\mathcal{L}_k\{\mathbf{U}_b, Re\}\mathbf{u} = \mathbf{U}_b \cdot \nabla_k \mathbf{u} + \mathbf{u} \cdot \nabla_k \mathbf{U}_b - \frac{1}{Re}\boldsymbol{\Delta}_k \mathbf{u} \;, \tag{2.4}$$

and $\boldsymbol{\Delta}_k \equiv \nabla_k \cdot \nabla_k$ is the Fourier-transformed Laplacian operator. In the Floquet stability analysis the linearised flow field $\mathbf{q} = \{\mathbf{u}, p\}$ is further assumed to have the following modal

form:

$$\mathbf{q}(x, y, k, t) = \hat{\mathbf{q}}(x, y, k, t) \exp(\sigma t) \tag{2.5}$$

where σ is the Floquet exponent while $\hat{\mathbf{q}} = \{\hat{\mathbf{u}}, \hat{p}\}$ is a non-trivial periodic field, with the same period T of the base flow, i.e. $(\hat{\mathbf{q}}(x, y, k, t + T) = \hat{\mathbf{q}}(x, y, k, t))$.

Substituting the modal form of the disturbance, (2.5), in (2.3) it is found that $\hat{\mathbf{q}}$ satisfies the following set of equations

$$\frac{\partial \hat{\mathbf{u}}}{\partial t} + \sigma \hat{\mathbf{u}} + L_k\{\mathbf{U}_b, Re\}\hat{\mathbf{u}} + \nabla_k \hat{p} = \mathbf{0} \tag{2.6a}$$

$$\nabla_k \cdot \hat{\mathbf{u}} = 0. \tag{2.6b}$$

along with homogeneous boundary conditions on the cylinder surface and appropriate far-field radiation conditions. This implies that, far enough from the cylinder, the perturbation behaves locally as an outgoing plane wave. While this last requirement enforces the correct causality relation, it does not generally imply that the disturbance vanishes at infinity. For the cylinder case, however, the spreading of the wake with the resulting attenuation of the vorticity and the rapid decay of the outer potential field produce a reduction of the perturbation amplitude with the radial distance. Consequently, the far-field conditions may be formulated as

$$\hat{\mathbf{q}} = \{\hat{\mathbf{u}}, \hat{p}\} \;\rightarrow\; \{\mathbf{0}, 0\} \qquad \text{as} \quad r \rightarrow \infty. \tag{2.7}$$

The system of equations (2.6) along with the above boundary conditions and the periodicity requirement for the solution $\hat{\mathbf{q}}$ is an eigenvalue problem for σ. The Floquet multipliers μ, which are the eigenvalues of the Floquet transition operator, are related to the Floquet exponents σ by the expression $\mu = \exp(\sigma T)$. By inspecting the modal form in equation (2.5) it is clear that the base flow becomes unstable whenever there exists a Floquet multiplier such that $Re(\mu) > 1$ ($Re(\cdot)$ indicating the real part of a complex number) or, equivalently, a Floquet exponent, such that $Re(\sigma) > 0$.

3. Sensitivity to a localized perturbation of the base flow

We start considering the unperturbed stability problem, which is composed of two sets of equations, (i) those governing the base flow, which is 2D and periodic in time:

$$\frac{\partial \mathbf{U}_b}{\partial t} + \mathbf{U}_b \cdot \nabla \mathbf{U}_b + \nabla P_b - \frac{1}{Re}\boldsymbol{\Delta}\mathbf{U}_b = \mathbf{0} \tag{3.1a}$$

$$\nabla \cdot \mathbf{U}_b = 0 \tag{3.1b}$$

and (ii) equations (2.6) which are the eigenvalue problem resulting from the Floquet stability analysis of the time-periodic baseflow. At difference with the analysis considered in Giannetti *et al.* (2010) and briefly recalled in section 4, where the effects of a perturbation of the sole disturbance equations is investigated, we now study the sensitivity of a selected Floquet exponent when a perturbation is applied to the base flow equations. In particular let us consider a generic 2D linear structural perturbation $\{\delta\mathbf{H}, \delta R\}$ acting on the base-flow equations. As a consequence, the base-flow field $\{\mathbf{U}_b, P_b\}$ changes in $\{\mathbf{U}_b + \delta\mathbf{u}_b, P_b + \delta p_b\}$ as shown in the following equations:

$$\frac{\partial \mathbf{U}_b + \delta\mathbf{u}_b}{\partial t} + (\mathbf{U}_b + \delta\mathbf{u}_b) \cdot \nabla(\mathbf{U}_b + \delta\mathbf{u}_b) + \nabla(\delta\mathbf{p}_b) - \frac{1}{Re}\boldsymbol{\Delta}(\mathbf{U}_b + \delta\mathbf{u}_b) = \delta\mathbf{H} \tag{3.2a}$$

$$\nabla \cdot (\mathbf{U}_b + \delta\mathbf{u}_b) = \delta R \tag{3.2b}$$

Besides directly changing the base flow, such a perturbation also affects the stability equations through a modification of the Linearised Navier Stokes (LNS) operator L_k induced by the variation $\delta\mathbf{u}_b$ of the base-flow velocity. In the following analysis we assume that the perturbations are weak enough to produce only a small change of the base flow and of the stability equations, so that a linearised analysis can be carried out. Consequently, we expand the results around the unperturbed state $\{\mathbf{U}_b, P_b\}$ and the unperturbed modal disturbance $\{\hat{\mathbf{u}}, \hat{p}\}$ (see Eq. (2.5)) by considering a small perturbation of the base flow ($\{\delta\mathbf{u}_b, \delta p_b\}$) and the induced perturbation of the disturbance ($\{\delta\hat{\mathbf{u}}, \delta\hat{p}\}$). In order to avoid secular effects in the perturbation analysis, it is convenient to introduce a rescaled time $\tau = t/T$, T being the period of the unperturbed base flow. Note that, as a consequence of the perturbation of the base flow, the period T also changes by an amount δT. Linearising equations (3.2) with respect to the perturbations $\{\delta\mathbf{u}_b, \delta p_b\}$ and using the rescaled time τ we obtain the following linearised equations for the base flow perturbation:

$$\frac{1}{T}\frac{\partial \delta\mathbf{u}_b}{\partial \tau} + \mathsf{L}_0\{\mathbf{U}_b Re\}\ \delta\mathbf{u}_b + \nabla_0\ \delta p_b = \frac{\delta T}{T^2}\ \frac{\partial \mathbf{U}_b}{\partial \tau} +\ \delta\mathsf{H}(\mathbf{U}_b, P_b) \tag{3.3a}$$

$$\nabla_0 \cdot \delta\mathbf{u}_b = \delta R(\mathbf{U}_b, P_b) \tag{3.3b}$$

where L_0 is the LNS operator computed for $k = 0$. The Floquet stability equations (2.6) is modified as a consequence of the base flow perturbation such that the perturbations $\delta\hat{\mathbf{u}}$, $\delta\hat{p}$ and $\delta\sigma$ are related together by the following linearised equations

$$\frac{1}{T}\frac{\partial \delta\hat{\mathbf{u}}}{\partial \tau} + \sigma\,\delta\hat{\mathbf{u}} + \mathsf{L}_k\{\mathbf{U}_b, Re\}\delta\hat{\mathbf{u}} + \frac{\partial \mathsf{L}_k}{\partial \mathbf{U}_b}\{\delta\mathbf{u}_b\}\hat{\mathbf{u}} + \nabla_k\,\delta\hat{p} = \frac{\delta T}{T^2}\frac{\partial \hat{\mathbf{u}}}{\partial \tau} - \delta\sigma\ \hat{\mathbf{u}} \tag{3.4a}$$

$$\nabla_k \cdot \delta\hat{\mathbf{u}} = 0. \tag{3.4b}$$

where the operator formally indicated by the term $\frac{\partial \mathsf{L}_k}{\partial \mathbf{U}_b}$ represent the change of the LNS operator L_k due to a small change of the base flow and is defined as

$$\frac{\partial \mathsf{L}_k\{\mathbf{U}_b\, Re\}}{\partial \mathbf{U}_b}\{\delta\mathbf{u}_b\}\hat{\mathbf{u}} = \delta\mathbf{u}_b \cdot \nabla_k\hat{\mathbf{u}} + \hat{\mathbf{u}} \cdot \nabla_k\delta\mathbf{u}_b \tag{3.5}$$

Equations (3.4) are a set of forced equations with periodic coefficients. We thus have to enforce compatibility conditions in order to guarantee the existence of periodic solutions which are those of interest here. In order to derive the compatibility conditions and express both the variation of the period T and of the Floquet exponent σ induced by the considered perturbation we derive a generalised Lagrange identity for the system of equations describing the perturbation problem, i.e. equations (3.3) and (3.4).

We start by scalarly multiplying equations (3.3) and (3.4) by a set of yet unspecified functions $(\mathbf{f}_b^+, m_b^+)$ and $(\mathbf{f}^+, m^+)$ (the adjoints fields), respectively, summing together the result and integrating both in space and time. The following identity is obtained as a

result:

$$\int_0^1\int_{\mathcal{D}}\left[\left(\frac{\delta T}{T^2}\frac{\partial \mathbf{U}_b}{\partial \tau}+\delta H(\mathbf{U}_b,P_b)\right)\cdot\mathbf{f}_b^+ + \delta R(\mathbf{U}_b,P_b)\ m_b^+\right]\mathrm{d}\mathcal{D}\,\mathrm{d}\tau+$$
$$\int_0^1\int_{\mathcal{D}}\left[\left(\frac{\delta T}{T^2}\frac{\partial \hat{\mathbf{u}}}{\partial \tau}-\delta\sigma\,\hat{\mathbf{u}}\right)\cdot\hat{\mathbf{f}}^+\right]\mathrm{d}\mathcal{D}\,\mathrm{d}\tau=$$
$$\int_0^1\int_{\mathcal{D}}\left[\left(\frac{1}{T}\frac{\partial \delta\mathbf{u}_b}{\partial \tau}+L_0\{\mathbf{U}_b,Re\}\delta\mathbf{u}_b+\nabla_0\,\delta p_b\right)\cdot\mathbf{f}_b^+ + (\nabla_0\cdot\delta\mathbf{u}_b)\ m_b^+\right]\mathrm{d}\mathcal{D}\,\mathrm{d}\tau+$$
$$\int_0^1\int_{\mathcal{D}}\left[\left(\frac{1}{T}\frac{\partial \delta\hat{\mathbf{u}}}{\partial t}+\sigma\,\delta\hat{\mathbf{u}}+L_k\{\mathbf{U}_b,Re\}\delta\hat{\mathbf{u}}+\frac{\partial L_k}{\partial \mathbf{U}_b}\{\delta\mathbf{u}_b\}\hat{\mathbf{u}}+\nabla_k\delta\hat{p}\right)\cdot\hat{\mathbf{f}}^+ + (\nabla_k\cdot\hat{\mathbf{u}})\ \hat{m}^+\right]\mathrm{d}\mathcal{D}\,\mathrm{d}\tau \tag{3.6}$$

As standard, integration by parts and the divergence theorem are used to shift the action of the differential operators in equation (3.6) from the flow fields to the adjoint fields $\mathbf{f}_b^+, m_b^+, \mathbf{f}^+, m^+$. As a result we have a different identity which is equivalent to equation (3.6) and also contains boundary integrals. The new version of the identity writes as

$$\int_0^1\int_{\mathcal{D}}\left[\left(\frac{\delta T}{T^2}\frac{\partial \mathbf{U}_b}{\partial \tau}+\delta H(\mathbf{U}_b,P_b)\right)\cdot\mathbf{f}_b^+ + \delta R(\mathbf{U}_b,P_b)\ m_b^+\right]\mathrm{d}\mathcal{D}\,\mathrm{d}\tau+$$
$$\int_0^1\int_{\mathcal{D}}\left[\left(\frac{\delta T}{T^2}\frac{\partial \hat{\mathbf{u}}}{\partial \tau}-\delta\sigma\,\hat{\mathbf{u}}\right)\cdot\hat{\mathbf{f}}^+\right]\mathrm{d}\mathcal{D}\,\mathrm{d}\tau=$$
$$\underbrace{-\int_0^1\int_{\mathcal{D}}\left[\delta\mathbf{u}_b\cdot\left(\frac{1}{T}\frac{\partial \mathbf{f}_b^+}{\partial \tau}+L_0^+\{\mathbf{U}_b,Re\}\mathbf{f}_b^+ + \nabla_0\,m_b^+ + \nabla_k\hat{\mathbf{u}}\cdot\hat{\mathbf{f}}^+ - \hat{\mathbf{u}}\cdot\nabla_k\hat{\mathbf{f}}^+\right) + p_b\ \left(\nabla_0\cdot\mathbf{f}_b^+\right)\right]\mathrm{d}\mathcal{D}\,\mathrm{d}\tau}_{(A)}$$
$$\underbrace{-\int_0^1\int_{\mathcal{D}}\left[\delta\hat{\mathbf{u}}\cdot\left(\frac{1}{T}\frac{\partial \hat{\mathbf{f}}^+}{\partial \tau}-\sigma\,\hat{\mathbf{f}}^+ + L_k^+\{\mathbf{U}_b,Re\}\hat{\mathbf{f}}^+ + \nabla_k\hat{m}^+\right) + \delta\hat{p}\ \left(\nabla_k\cdot\hat{\mathbf{f}}^+\right)\right]\mathrm{d}\mathcal{D}\,\mathrm{d}\tau}_{(B)}$$
$$\underbrace{\frac{1}{T}\int_{\mathcal{D}}\left[\delta\mathbf{u}_b\cdot\mathbf{f}_b^+\right]_{\tau=0}^{\tau=1}\mathrm{d}\mathcal{D} + \frac{1}{T}\int_{\mathcal{D}}\left[\delta\hat{\mathbf{u}}\cdot\hat{\mathbf{f}}^+\right]_{\tau=0}^{\tau=1}\mathrm{d}\mathcal{D}}_{(C)} +$$
$$\underbrace{\int_0^1\oint_{\mathcal{D}}\mathbf{J}(\delta\mathbf{q}_b,\mathbf{g}_b^+)\cdot\mathbf{n}\mathrm{d}s\mathrm{d}\tau}_{(D)} + \underbrace{\int_0^1\oint_{\mathcal{D}}\mathbf{J}(\delta\hat{\mathbf{q}},\hat{\mathbf{g}}^+)\cdot\mathbf{n}\mathrm{d}s\mathrm{d}\tau}_{(E)} + \underbrace{\int_0^1\oint_{\mathcal{D}}\left[\left(\delta\mathbf{u}_b\cdot\hat{\mathbf{f}}^+\right)\hat{\mathbf{u}}\right]\cdot\mathbf{n}\mathrm{d}s\mathrm{d}\tau}_{(F)} \tag{3.7}$$

In this expression $\mathbf{J}(\mathbf{q},\mathbf{g}^+)$ is the "bilinear concomitant", which is defined for two generic fields $\mathbf{q}=\{\mathbf{u},p\}$ and $\mathbf{g}^+=\{\mathbf{f}^+,m^+\}$ as follows

$$\mathbf{J}(\mathbf{q},\mathbf{g}^+)=\mathbf{U}_b(\mathbf{u}\cdot\mathbf{f}^+)+\frac{1}{Re}\left(\nabla_k\mathbf{f}^+\cdot\mathbf{u}-\nabla_k\mathbf{u}\cdot\mathbf{f}^+\right)+m^+\ \mathbf{u}+p\ \mathbf{f}^+ \tag{3.8}$$

and L_k^+ is the adjoint linearised Navier-Stokes operator with wavenumber k defined as

follows:

$$L_k^+\{\mathbf{U}_b, Re\}\mathbf{f}^+ = \mathbf{U}_b \cdot \nabla_k \mathbf{f}^+ - \nabla_k \mathbf{U}_b \cdot \mathbf{f}^+ + \frac{1}{Re}\boldsymbol{\Delta}_k \mathbf{f}^+. \tag{3.9}$$

As for the LNS operator, the subscript $_0$ in L_k^+ indicate the contribution from the zero wavenumber components. In order to further simplify the identity (3.7) we assume that the field $(\mathbf{f}_b^+, m_b^+)$, which is the adjoint base-flow field, is a *periodic* solution of the following forced adjoint equations

$$\frac{1}{T}\frac{\partial \mathbf{f}_b^+}{\partial \tau} + L_0^+\{\mathbf{U}_b, Re\}\mathbf{f}_b^+ + \nabla_0 m_b^+ = -\nabla_k \hat{\mathbf{u}} \cdot \hat{\mathbf{f}}^+ + \hat{\mathbf{u}} \cdot \nabla_k \hat{\mathbf{f}}^+ \tag{3.10a}$$

$$\nabla_0 \cdot \mathbf{f}_b^+ = 0 \tag{3.10b}$$

In this way, term (A) in equation (3.7) vanishes. Analogously, term (B) also vanishes if we assume that the fields $(\hat{\mathbf{f}}^+, \hat{m}^+)$, which indicates the adjoint stability mode corresponding to the Floquet exponent σ, satisfy the following equations:

$$\frac{1}{T}\frac{\partial \hat{\mathbf{f}}^+}{\partial \tau} + L_k^+\{\mathbf{U}_b, Re\}\hat{\mathbf{f}}^+ + \nabla_k \hat{m}^+ - \sigma\, \hat{\mathbf{f}}^+ = \mathbf{0} \tag{3.11a}$$

$$\nabla_k \cdot \hat{\mathbf{f}}^+ = 0. \tag{3.11b}$$

Assuming that the solutions of equations (3.10) and (3.11) are periodic in time with the same period T of the unperturbed base flow also term (C) vanishes. Finally, boundary conditions for the adjoint flow fields can be found so as to make terms (D), (E) and (F) to vanish. In the continuous problem these conditions imply that the adjoint flow fields vanish on the cylinder surface and decay at infinity. When the problem is discretised by a numerical method, numerical boundary conditions can be imposed so that terms (D), (E) and (F) vanish at discrete level. However, we will see that with the selected numerical approach described in section 5 the boundary conditions for the adjoint problems are automatically taken into account at the discrete level.

After the assumptions described above equation (3.7) finally becomes

$$\int_0^1 \int_{\mathcal{D}} \left[\left(\frac{\delta T}{T^2}\frac{\partial \mathbf{U}_b}{\partial \tau} + \delta H(\mathbf{U}_b, P_b) \right) \cdot \mathbf{f}_b^+ + \delta R(\mathbf{U}_b, P_b)\; m_b^+ \right] \mathrm{d}\mathcal{D}\, \mathrm{d}\tau + \int_0^1 \int_{\mathcal{D}} \left[\left(\frac{\delta T}{T^2}\frac{\partial \hat{\mathbf{u}}}{\partial \tau} - \delta\sigma\, \hat{\mathbf{u}} \right) \cdot \hat{\mathbf{f}}^+ \right] \mathrm{d}\mathcal{D}\, \mathrm{d}\tau = 0 \tag{3.12}$$

Note that in equation (3.12) all the perturbation terms have disappeared with the exception of δT and $\delta\sigma$. Solving for $\delta\sigma$ we obtain

$$\delta\sigma = \frac{\displaystyle\int_0^1 \int_{\mathcal{D}} \left[\delta H(\mathbf{U}_b, P_b) \cdot \mathbf{f}_b^+ + \delta R(\mathbf{U}_b, P_b)\; m_b^+ \right] \mathrm{d}\mathcal{D}\, \mathrm{d}\tau + \int_0^1 \int_{\mathcal{D}} \frac{\delta T}{T^2} \left[\frac{\partial \mathbf{U}_b}{\partial \tau} \cdot \mathbf{f}_b^+ + \frac{\partial \hat{\mathbf{u}}}{\partial \tau} \cdot \hat{\mathbf{f}}^+ \right] \mathrm{d}\mathcal{D}\, \mathrm{d}\tau}{\displaystyle\int_0^1 \int_{\mathcal{D}} \hat{\mathbf{u}} \cdot \hat{\mathbf{f}}^+ \, \mathrm{d}\mathcal{D}\, \mathrm{d}\tau} \tag{3.13}$$

Equation (3.13) is still not usable in practice to estimate $\delta\sigma$ as a function of the generic perturbations δH and δR because the variation δT of the base flow period is still unknown. Another problem in its practical use seems to arise from the fact that the solution of the forced system in equation (3.10), $(\hat{\mathbf{f}}_b, \hat{m}_b)$, is not unique but nevertheless is used in equation (3.13) so as to estimate $\delta\sigma$. Indeed, we can always add to a particular solution

of equation (3.10) a solution of the associated homogeneous system and the resulting sum is still a solution of the forced problem. In order to solve this ambiguity let us define the field $(\{\mathbf{f}_{bh}^+, m_{bf}^+\})$ as a solution of the homogeneous system associated to equation (3.10):

$$\frac{1}{T}\frac{\partial \mathbf{f}_{bh}^+}{\partial \tau} + \mathsf{L}_0^+\{\mathbf{U}_b, Re\}\mathbf{f}_{bh}^+ + \nabla_0 m_{bh}^+ = \mathbf{0} \tag{3.14a}$$

$$\nabla_0 \cdot \mathbf{f}_{bh}^+ = 0 \tag{3.14b}$$

and let us write the general solution of the forced problem as a superposition of a particular solution $(_{bp})$ and of the homogeneous $(_{bh})$ solution as

$$\mathbf{f}_b^+ = \mathbf{f}_{bp}^+ + \eta\,\mathbf{f}_{bh}^+ \tag{3.15a}$$

$$m_b^+ = m_{bp}^+ + \eta\, m_{bh}^+ \tag{3.15b}$$

with η being an undetermined coefficient. Substituting equation (3.15) into equation (3.13) we obtain the following expression for $\delta\sigma$:

$$\delta\sigma = \frac{\displaystyle\int_0^1\int_{\mathcal{D}}\left[\delta H(\mathbf{U}_b,P_b)\cdot(\mathbf{f}_{bp}^+ + \eta\mathbf{f}_{bh}^+) + \delta R(\mathbf{U}_b,P_b)\;(m_{bp}^+ + \eta m_{bh}^+)\right]\mathrm{d}\mathcal{D}\,\mathrm{d}\tau}{\displaystyle\int_0^1\int_{\mathcal{D}}\hat{\mathbf{u}}\cdot\hat{\mathbf{f}}^+\;\mathrm{d}\mathcal{D}\,\mathrm{d}\tau} + \frac{\displaystyle\int_0^1\int_{\mathcal{D}}\frac{\delta T}{T^2}\left[\frac{\partial \mathbf{U}_b}{\partial\tau}\cdot(\mathbf{f}_{bp}^+ + \eta\mathbf{f}_{bp}^+) + \frac{\partial \mathbf{u}}{\partial\tau}\cdot\mathbf{f}^+\right]\mathrm{d}\mathcal{D}\,\mathrm{d}\tau}{\displaystyle\int_0^1\int_{\mathcal{D}}\hat{\mathbf{u}}\cdot\hat{\mathbf{f}}^+\;\mathrm{d}\mathcal{D}\,\mathrm{d}\tau} \tag{3.16}$$

Note that in this equation the variation of the period δT is still undetermined. Furthermore, written in this way, it might seem that the variation $\delta\sigma$ of the considered Floquet exponent depends on the particular choice of the coefficient η. Recall however that equation (3.3) which governs the evolution of the 2D perturbation induced by the localised perturbation is a forced equation with periodic coefficients. In particular the forcing terms are those on the RHS of equations (3.3a) and (3.3b). The solution to this system of equations is also *periodic* provided that a compatibility condition is imposed, which can be derived by writing a related Green identity or by imposing the Fredholm alternative. The Fredholm alternative requires the forcing term to be orthogonal to the homogeneous solution of the adjoint equations:

$$\int_0^1\int_{\mathcal{D}}\left[\frac{\delta T}{T^2}\frac{\partial \mathbf{U}_b}{\partial\tau} + \delta H(\mathbf{U}_b,P_b)\right]\cdot\mathbf{f}_{bh}^+ + \delta R(\mathbf{U}_b,P_b)\;m_{bh}^+\,\mathrm{d}\mathcal{D}\,\mathrm{d}\tau = 0 \tag{3.17}$$

Condition in equation (3.17) has two important implications. Firstly, that the solution for $\delta\sigma$ given in equation (3.16) is independent of the value of η. Secondly, equation (3.17) can be solved for $\delta T/T^2$ giving the following result

$$\frac{\delta T}{T^2} = -\delta S_t = -\frac{\displaystyle\int_0^1\int_{\mathcal{D}}\delta H(\mathbf{U}_b,P_b)\cdot\mathbf{f}_{bh}^+ + \delta R(\mathbf{U}_b,P_b)\;m_{bh}^+\,\mathrm{d}\mathcal{D}\,\mathrm{d}\tau}{\displaystyle\int_0^1\int_{\mathcal{D}}\frac{\partial \mathbf{U}_b}{\partial\tau}\cdot\mathbf{f}_{bh}^+\,\mathrm{d}\mathcal{D}\,\mathrm{d}\tau} \tag{3.18}$$

where St is the Strouhal number associated to vortex shedding, i.e. its normalised frequency. Since all quantities on the RHS are known, equation (3.18) allows the estimation

of δT as a function of the generic perturbations δH and δR of the base flow. If we reintroduce time t in equation (3.18) we finally obtain the following equivalent expression for the variation δT:

$$\frac{\delta T}{T} = -\frac{\displaystyle\int_0^T \int_{\mathcal{D}} \delta H(\mathbf{U}_b, P_b) \cdot \mathbf{f}_{bh}^{+} + \delta R(\mathbf{U}_b, P_b)\; m_{bh}^{+}\, \mathrm{d}\mathcal{D}\, \mathrm{d}t}{\displaystyle\int_0^T \int_{\mathcal{D}} \frac{\partial \mathbf{U}_b}{\partial t} \cdot \mathbf{f}_{bh}^{+}\, \mathrm{d}\mathcal{D}\, \mathrm{d}t}. \tag{3.19}$$

Once it has been shown that the arbitrary constant η does not affect $\delta\sigma$, it is possible to properly choose its value so as to further simplify equation (3.16), which is now usable for estimating $\delta\sigma$ since δT is now known from equation (3.18) or, equivalently, from equation (3.19). In particular, it is possible to choose a particular value of η in order to make the second integral in equation (3.16) null as follow:

$$\eta = \frac{\displaystyle\int_0^1 \int_{\mathcal{D}} \frac{\partial \mathbf{U}_b}{\partial \tau} \cdot \mathbf{f}_{bp}^{+} + \frac{\partial \mathbf{u}}{\partial \tau} \cdot \mathbf{f}^{+} \mathrm{d}\mathcal{D}\, \mathrm{d}\tau}{\displaystyle\int_0^1 \int_{\mathcal{D}} \frac{\partial \mathbf{U}_b}{\partial \tau} \cdot \mathbf{f}_{bh}^{+} \mathrm{d}\mathcal{D}\, \mathrm{d}\tau} \tag{3.20}$$

If we rewrite equation (3.16) with η given by equation (3.20) and we reintroduce the unscaled time t we finally obtain the following equation, which allows the estimation of $\delta\sigma$ as a function of the generic perturbations δH and δR:

$$\delta\sigma = \frac{\displaystyle\int_0^T \int_{\mathcal{D}} \left[\delta H(\mathbf{U}_b, P_b) \cdot \mathbf{f}_b^{+} + \delta R(\mathbf{U}_b, P_b)\; m_b^{+} \right] \mathrm{d}\mathcal{D}\, \mathrm{d}t}{\displaystyle\int_0^T \int_{\mathcal{D}} \hat{\mathbf{u}} \cdot \hat{\mathbf{f}}^{+}\, \mathrm{d}\mathcal{D}\, \mathrm{d}t}. \tag{3.21}$$

Note that when the Floquet exponent σ is real valued (both positive or negative) the associated eigenmode is real, too. In this case $\delta\sigma$ is also real indicating that only the growth rate of the mode is affected by the structural perturbation. On the other hand, when σ is complex valued $\delta\sigma$ generally has an imaginary part different form zero and the structural perturbation affects both the real and the imaginary parts of σ.

If we further assume $\delta R(\mathbf{U}_b, P_b) = 0$, i.e. we do not perturb the continuity equation mimicking a local addition/subtraction of mass, but we only perturb the momentum equation with δH, equation (3.21) further simplifies to

$$\delta\sigma = \frac{\displaystyle\int_0^1 \int_{\mathcal{D}} \delta H(\mathbf{U}_b, P_b) \cdot \mathbf{f}_b^{+}\, \mathrm{d}\mathcal{D}\, \mathrm{d}\tau}{\displaystyle\int_0^1 \int_{\mathcal{D}} \hat{\mathbf{u}} \cdot \hat{\mathbf{f}}^{+}\, \mathrm{d}\mathcal{D}\, \mathrm{d}\tau} \tag{3.22}$$

Summarising, the analysis carried out in this section allows the estimation of the variation of (i) the vortex shedding period (or, equivalently, of the associated Strouhal number) and of (ii) the Floquet exponent associated to an identified instability, induced by a generic distributed perturbation of the momentum and continuity equations governing the dynamics of time-periodic base flow.

4. Sensitivity analysis to a localised velocity-force feedback

The synthetic results obtained in the previous section, in particular equations (3.18) and (3.22), are used here in order to quantify the effects on the vortex shedding frequency and on the Floquet exponent related to either mode A or mode B instabilities that are induced by a particular perturbation, i.e. a localised velocity-force feedback acting on the momentum equations. This particular perturbation is significant because a localised velocity-force feedback can model the presence of a small control body in the flow, as often done in the literature (see for instance Camarri (2015) for a review). In the case of the three dimensional wake past a circular cylinder, for instance, it is an appropriate model to represent the control excerted by a small wire, with the axis parallel to the cylinder axis, positioned in the wake, as done in the experiments documented in Zhang *et al.* (1995). Thus, appropriately built sensitivity maps for the considered velocity-force perturbation can be used as control maps so as to predict the effect of a small control wire on the three dimensional stability characteristics of the wake. In this second case it is however necessary to take into account the action of the perturbation when this acts both on the base flow, as investigated in section 3, and on the linearised flow equations, as already done in Giannetti *et al.* (2010).

When a localised velocity-force feedback acting on the sole base flow is considered, the generic perturbation δH assumes the form of a local reaction force proportional to the local velocity field:

$$\delta H(\mathbf{U}_b, P_b) = \delta(x - x_0, y - y_0)\ C_1 \cdot \mathbf{U}_b \quad , \tag{4.1}$$

where C_1 is a generic constant feedback matrix, (x_0, y_0) are the coordinates of the point where the feedback acts and $\delta(x - x_0, y - y_0)$ is the Dirac delta function.

Substituting (4.1) in (3.18) it is possible to estimate the effect of the considered perturbation on the vortex shedding frequency:

$$\delta S_t = \frac{\displaystyle\int_0^1 \int_{\mathcal{D}} \delta(x - x_0, y - y_0)\ C_1 \cdot \mathbf{U}_b \cdot \mathbf{f}_{bh}^{+}\, \mathrm{d}\mathcal{D}\, \mathrm{d}\tau}{\displaystyle\int_0^1 \int_{\mathcal{D}} \frac{\partial \mathbf{U}_b}{\partial \tau} \cdot \mathbf{f}_{bh}^{+}\, \mathrm{d}\mathcal{D}\, \mathrm{d}\tau} = C_1 : S_s(x_0, y_0) \tag{4.2}$$

where S_s is the sensitivity tensor field of the vortex shedding frequency (Strouhal number) with respect to the localised perturbation in (4.1), and it is defined as follows:

$$S_s(x, y) = \frac{\displaystyle\int_0^T \mathbf{U}_b(x, y, k, t)\ \mathbf{f}_{bh}^{+}(x, y, k, t)\ \mathrm{d}t}{\displaystyle\int_0^1 \int_{\mathcal{D}} \frac{\partial \mathbf{U}_b}{\partial \tau} \cdot \mathbf{f}_{bh}^{+}\, \mathrm{d}\mathcal{D}\, \mathrm{d}\tau} \tag{4.3}$$

An analogous result can be obtained for the Floquet exponent of the instability by substituting (4.1) in (3.22):

$$\delta\sigma = \frac{\displaystyle\int_0^T \int_D \delta(x - x_0, y - y_0)\ C_1 \cdot \mathbf{U}_b \cdot \tilde{\mathbf{f}}_b^{+}\ \mathrm{d}S\ \mathrm{d}t}{\displaystyle\int_0^T \int_{\mathcal{D}} \hat{\mathbf{u}} \cdot \hat{\mathbf{f}}^{+}\ \mathrm{d}S\ \mathrm{d}t} = C_1 : S_b(x_0, y_0, k) \tag{4.4}$$

In this case the tensor S_b is the sensitivity tensor field of the Floquet exponent σ with

respect to the localised perturbation in (4.1), and it is defined as follows:

$$S_b(x,y,k) = \frac{\displaystyle\int_0^T \mathbf{U}_b(x,y,k,t)\ \tilde{\mathbf{f}}_b(x,y,k,t)\ \mathrm{d}t}{\displaystyle\int_0^T \int_{\mathcal{D}} \hat{\mathbf{u}}\cdot\hat{\mathbf{f}}^{+}\ \mathrm{d}S\ \mathrm{d}t} \quad . \tag{4.5}$$

As already stated above, if a localised velocity-force feedback of the same type of (4.1) is applied to the total velocity field and not only to the base flow, another additional sensitivity tensor arises (S_I) for quantifying the variation of the Floquet exponent, whose effect must be summed to that of S_b. This tensor arises from the sensitivity analysis of the sole linearised stability equations, which is proposed and carried out in Giannetti *et al.* (2010). Summarising the results of that paper, we consider a perturbation of the same type of (4.1) but acting only on the linearised flow equations:

$$\delta H_L(\mathbf{u},p) = \delta(x-x_0,y-y_0)\ C_1\cdot\mathbf{u} \quad , \tag{4.6}$$

the effect of such a perturbation on the Floquet exponent can be quantified as follows:

$$\delta\sigma = \frac{\displaystyle\int_t^{t+T}\int_D \mathbf{f}^{+}\cdot\delta(x-x_0,y-y_0)\ C_1\cdot\mathbf{u}\ \mathrm{d}S\ \mathrm{d}t}{\displaystyle\int_t^{t+T}\int_{\mathcal{D}} \mathbf{f}^{+}\cdot\mathbf{u}\ \mathrm{d}S\ \mathrm{d}t} = C_1 : S_I(x_0,y_0,k) \tag{4.7}$$

where S_I is the structural sensitivity tensor of the Floquet mode, defined as

$$S_I(x,y,k) = \frac{\displaystyle\int_t^{t+T} \mathbf{f}^{+}(x,y,k,t)\ \mathbf{u}(x,y,k,t)\ \mathrm{d}t}{\displaystyle\int_t^{t+T}\int_{\mathcal{D}} \mathbf{f}^{+}\cdot\mathbf{u}\ \mathrm{d}S\ \mathrm{d}t} \quad . \tag{4.8}$$

Since the analysis carried out here is linear, if we consider a localised velocity-force feedback acting on the whole velocity field $\mathbf{U}$:

$$\delta H_T = \delta(x-x_0,y-y_0)\ C_1\cdot\mathbf{U} \quad , \tag{4.9}$$

the effect of such perturbation on the Floquet exponent of an identified instability is given as the sum of the two contributions, i.e. the one coming from perturbation (4.1) and one from perturbation (4.6):

$$\delta\sigma = C_1 : S_{tot} \tag{4.10}$$

where the total sensitivity tensor field S_{tot} is given as follows

$$S_{tot} = S_I + S_b. \tag{4.11}$$

We stress out that the two components of the total sensitivity tensor serve for different purposes: the sensitivity S_I is appropriate to identify the driving mechanism of the global instability (the wavemaker) while both S_b and S_I are useful to develop passive control strategies for the secondary instability.

Finally, since the perturbation (4.6) on the linearised equations cannot have an influence on the vortex shedding frequency, the variation of frequency induced by perturbation (4.9) is the same as that induced by perturbation (4.1) and is given in equation (4.2).

5. Numerical Approach

In the present work the numerical simulation of the base flow, of the direct and adjoint Floquet problems and of the problem adjoint to the time-periodic base flow are all solved using an ad-hoc finite-difference code. The finite-difference code used here is the same of Giannetti *et al.* (2010). Its description is concisely given in this section, referring to the reference cited above for further details.

The spatial discretisation of the equations is carried out on a staggered grid using a classical second-order centred finite-difference scheme built starting from the conservative form of the equations. A non-uniform cartesian grid is used on a rectangular computational domain. Since the grid is non-conformal with the cylinder, on which a no-slip boundary condition is applied, second-order immersed-boundary (IBM) technique is used. The time discretization is carried out using the Rai & Moin (1991) scheme, i.e. a hybrid third-order Runge-Kutta/Crank-Nicolson scheme. This choice implies an explicit discretization of the convective terms while the remaining terms are implicitly discretized. Pressure is solved implicitly in a coupled way together with the velocity field. Linear systems arising at each time step are solved by the sparse LU algorithm implemented in the UMFPACK library Davis (2004). The linearised Navier-Stokes equations are solved by linearising the nonlinear solver described above at discrete level and by imposing appropriate homogeneous boundary conditions. Adjoint solvers are also obtained at discrete level starting from the direct solvers (discrete adjoint) so that the combined properties of direct and adjoint modes are verified to machine accuracy and the correct boundary conditions for the adjoint problems are automatically taken into account.

Concerning the simulation of the base flow, the 2D Navier-Stokes equations are advanced in time until a periodic solution is obtained. For the direct and adjoint Floquet stability analysis, a power method is used so as to identify the dominant Floquet modes and the associated multipliers, and at each step of the power method the linearised Navier-Stokes equations are solved over one vortex shedding period. The forced adjoint base-flow problem is solved with the same numerics of the direct stability problem.

In the present work we use the same size of the computational domain adopted by Giannetti *et al.* (2010) for the same problem. In order to obtain the base flow, we use a uniform velocity profile ($U = 1, V = 0$) at the inlet and on the later boundaries of the computational domain, and a convective outflow condition ($\frac{\partial V}{\partial x} = 0, -P + Re^{-1} 2 \frac{\partial U}{\partial x} = 0$) is imposed on the outlet. The boundary conditions for the linearised problem are simply derived from those adopted for the base flow computations. Thus, homogeneous Dirichlet conditions ($U = 0, V = 0$) are imposed on the inlet and on the lateral boundaries while the same convective condition is imposed on the outflow.

As concerns discretization in time, the time step is chosen in order to have about 500 points per shedding cycle. Both the computational domain and the spatio-temporal resolution are the same as those previously used in Giannetti *et al.* (2010). We refer to that paper for details concerning the validation of the code against the literature and for details on the grid-convergence tests and resolution.

For a complete validation of the results obtained by the sensitivity analysis, we have decided to use full 3D DNS simulations carried out with a completely different code. In this way it is possible to validate at the same time (i) the ad-hoc solvers that we have implemented, (ii) the numerical resolution adopted and (iii) the derivation of the sensitivity maps both as concerns the theory and the numerical implementation. To this purpose we used the open-source code Nek5000 (`https://nek5000.mcs.anl.gov`), which is a massively parallel code based on a spectral-element method (SEM), where the spatial discretisation of the domain is carried out using hexahedral elements. The code

employs langrangian finite elements based on Gauss-Lobatto-Legendre (GLL) quadrature points. The discretisation in time is carried out by a third-order backward differentiation formula (BDF3). In particular, the diffusive terms are treated implicitly in time, while a third order explicit extrapolation formula (EXT3) is considered for the convective terms. The computational domain for the present simulation is the same as that validated and used in Camarri *et al.* (2013) for the DNS of the flow past a circular cylinder up to a Reynolds number equal to 400. With reference to the cartesian system introduced previously (see the definition above), the inlet boundary is at $x_{inlet2} = -15\,D$, the lateral boundaries are located at $y_{lat2} = \pm 15\,D$ and the outflow is located at $x_{outlet2} = 35D$. Dirichlet boundary conditions are imposed on the inlet and lateral boundaries, forcing the undisturbed velocity field, while stress-free outflow conditions are imposed at the outlet boundary. Since three-dimensional simulations are carried out with focus on mode A, the domain extension L_z in the homogeneous direction z is taken approximately equal to $Lz \simeq 3.964D$, corresponding to a fundamental wavenumber k_z approximately equal to $k = 1.585$, and periodic boundary conditions are then applied along z. The three-dimensional grid is built by extruding a 2D grid made of approximately 1500 spectral elements the z direction. Two three-dimensional grids have been built, one using 16 spectral elements in the spanwise direction (globally 24000 elements for the 3D grid) and one using 5 elements (globally 7500 elements). It was observed that, for what concerns the vortex shedding frequency and the Floquet exponent computed by 3D DNS, the results obtained with the two different grids were almost identical, differences being not meaningful for the objectives of the present work. For this reason the results presented here are obtained on the coarser grid unless otherwise specified. The simulations have been carried out with a $P_N - P_{N-2}$ formulation for the stabilisation of spurious pressure modes, and the polynomial degree N used is $N = 6$. Dealiasing is applied to the convective non-linear term, which are thus computed with $N = 9$. Time step for advancing the simulation in time is fixed to $\Delta t = 5{\cdot}10^{-3}$, corresponding to a CFL number approximately equal to 0.35, which implies the use of about 1000 time steps for each shedding cycle.

As will be clear in the following, for the validity of DNS tests carried out here it is not important that we have a perfect matching between the results obtained with our finite-difference code and those obtained by Nek5000. Nevertheless we have carried out a cross comparison at $Re = 190$ so as to appreciate the accuracy of the 3D DNS simulations carried out by Nek5000. The Strouhal numbers obtained with the two codes, $St = 0.1971$ and $St = 0.1962$ (Nek5000), compare well, differences being of the order of 0.4% and compare well with the literature, for instance $St = 0.1954$ in Barkley & Henderson (1996). Concerning the Floquet multiplier for $k = 1.585$, the stability analysis obtained by the finite-difference code predicts $\mu \simeq 1.002$ while the same value estimated by 3D DNS is $\mu \simeq 1.009$, differences being of the order of 0.7%. In terms of estimated critical Reynolds number Re_{crA} for the onset of mode A, stability analysis estimates $Re_{crA} \simeq 189.77$ while with 3D DNS ($k = 1.585$) we obtain $Re_{crA} \simeq 189.71$, both values being in excellent agreement among them and with $Re_{crA} \simeq 188.5$ reported in Barkley & Henderson (1996).

6. Results

6.1. *Sensitivity analysis*

In the present section, we apply the proposed theoretical formalism in order to compute the sensitivity tensor fields defined in section 4 and to investigate their properties for the secondary instability of the cylinder wake. As shown in Barkley & Henderson (1996) ,

the critical Reynolds number and the wavenumber associated with mode A are $Re_{cr}^{A} \approx 189$ and $k_A \simeq 1.585$, while for mode B we have $Re_{cr}^{B} \approx 259$ and $k_B \simeq 7.640$. The stability analysis carried out here confirms these findings with a very good accuracy, as documented in Giannetti *et al.* (2010) and partially reported in section 5. In order to focus attention on modes A and B, two nearly marginally stable configurations have been considered here for carrying out the sensitivity analysis and for the derivation of the control maps. These two configurations are ($Re^A = 190$,$k_A = 1.585$) for mode A and ($Re^B = 260$,$k_B = 7.640$) for mode B. The same two configurations were considered in Giannetti *et al.* (2010) where the structural sensitivity analysis of the linearised stability equations is detailed leading to the computation and the analysis of tensor field S_l by the numerical evaluation of equation (4.8). In the present work we have computed the tensor field S_b evaluating numerically equation (4.5) and the tensor S_s in equation (4.3). Both tensor fields S_b and S_l contribute to the flow sensitivity with respect to a local velocity-force feedback perturbation acting on the total velocity field, in agreement with equation (4.10). In order to provide a synthetic view of the sensitivity tensors fields, we plot their spectral norm, which provides maps related to the maximum effect that a local velocity-force feedback can have on the Floquet exponent as shown by the following inequalities:

$$|\delta\sigma| = \|C_1 : S_{tot}\| \leq \|C_1\| \, \|S_{tot}\| = \|C_1\| \, \|S_b + S_l\| \leq \|C_1\| \, (\|S_b\| + \|S_l\|) \tag{6.1}$$

In particular, we report in figure 1 the spectral norm of the S_b obtained for modes A and B and in figure 2 the spectral norm of the S_l obtained in Giannetti *et al.* (2010) for the same two configurations. From the cited figures we note that the region where the spectral norm of S_b is significantly different from zero is localised in space in a region comprising the shear layers originating on the lateral sides of the cylinder and the recirculation region in the wake. A similar behaviour was observed by Luchini *et al.* (2009) for the sensitivity of the nonlinear saturated limit cycle. By comparison with the behaviour of S_l in space, it is possible to see that the regions where both are non-negligible is approximately the same in the wake, while S_b is also important on the shear layers, extending more in the y direction inside the region approximately comprised in $-0.6 \leq x \leq 1$. Moreover, in the case of mode B (see figure 1(b)) S_b is significant also upstream the cylinder at least up to $x = -2$. The same behaviour has been observed for the primary wake instability in Marquet *et al.* (2008). Figure 3 shows the sum of the spectral norms of S_b (figures 1) and of S_l (figures 2) for modes A and B. Despite analysing regions where the spectral norms are non negligible, it is also interesting to compare tensors S_b and S_l from a quantitative viewpoint. This can be done by comparing the values of the spectral norm of S_b in figure 1 to that of S_l in figure 2. This comparison shows that for mode A (see subfigures (a)) the variation of the Floquet exponent induced by the localised velocity-force feedback due to a change of the baseflow, represented by S_b, are of the same order of magnitude of those induced by the direct action of the perturbation on the dynamics of the three dimensional perturbations, represented by S_l. Conversely, as concerns mode B, variations induced by a change of the baseflow are dominant, and they are one order of magnitude larger than those related to S_l. In both cases the contribution of the variations of the baseflow is very important and must be taken into account if we want to use the present analysis for a quantitative prediction of possible passive controls of the secondary instability.

6.2. *Control maps*

In this subsection we focus on the idea of providing control maps, derived on the basis of the theoretical work illustrated in section 4, and thus using the sensitivity tensors defined there, so as to provide quantitative information on the possible control that can be

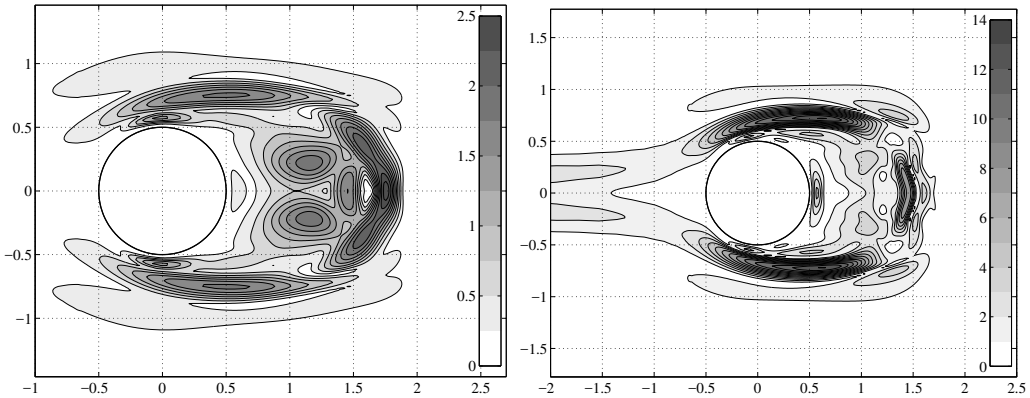

FIGURE 1. Contour plot of the spectral norm of the Base-flow Sensitivity tensor S_b: a) mode A ($Re = 190$, $k = 1.585$) and b) mode B ($Re = 260$, $k = 7.64$)

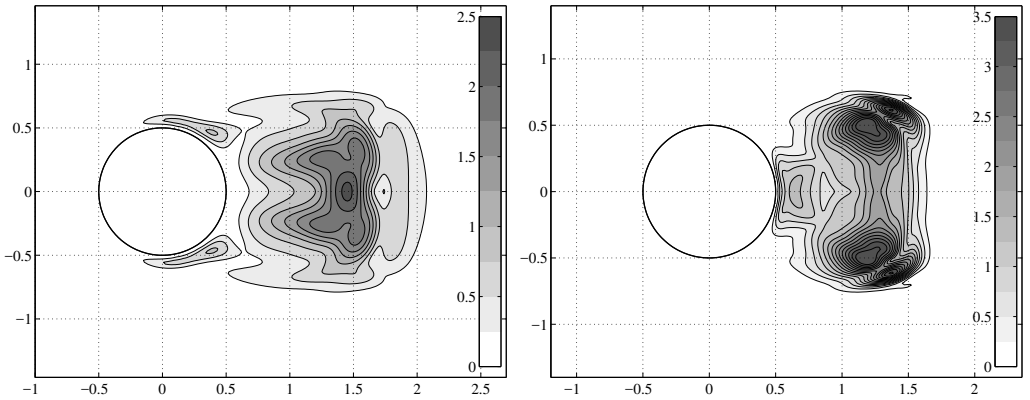

FIGURE 2. Spatial distribution of the spectral norm of the sensitivity tensor field S_l of the linearised stability equations, computed and reported in Giannetti *et al.* (2010): a) mode A ($Re = 190$, $k = 1.585$) and b) mode B ($Re = 260$, $k = 7.64$)

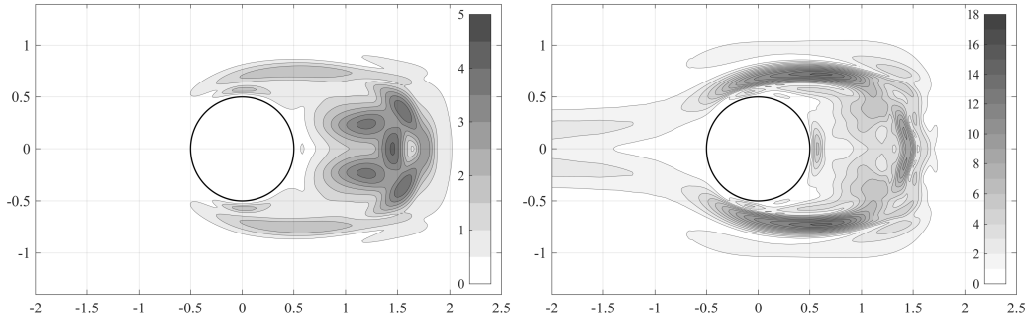

FIGURE 3. Field resulting from the sum of the spectral norms of the sensitivity tensor fields S_b and S_l: a) mode A ($Re = 190$, $k = 1.585$) and b) mode B ($Re = 260$, $k = 7.64$)

excerted by introducing a small wire in the flow with its axis parallel to the cylinder axis. An example of this kind of passive control is illustrated in the experiments documented in Zhang *et al.* (1995), where a small wire of diameter in the ratio of 1 : 160 with the cylinder diameter (initially used as a hydrogen-bubble wire for flow visualisation in

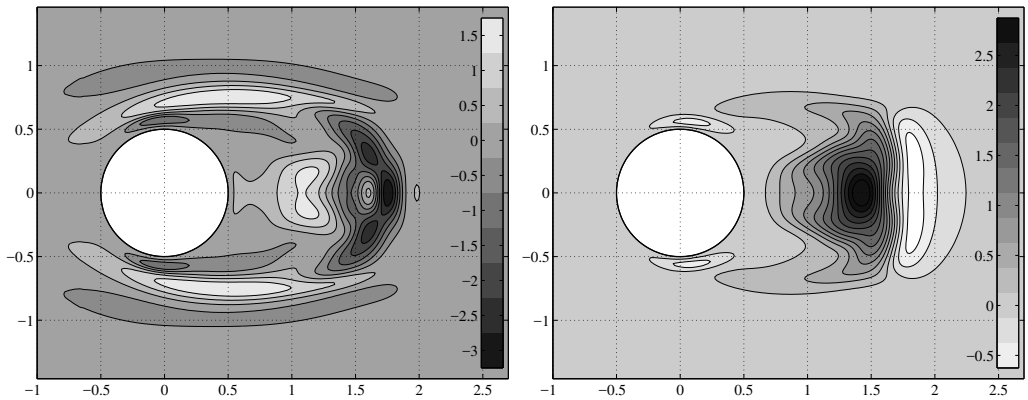

FIGURE 4. Mode A ($Re = 190$, $k = 1.585$): scalar fields (a) $\mathrm{Tr}\,(\boldsymbol{S}_b)$ and b) $\mathrm{Tr}\,(\boldsymbol{S}_l)$.)

water) was observed to interfere with the secondary instability of the wake past a circular cylinder so that, in precise positions, it could stabilise the wake otherwise unstable to three-dimensional instabilities.

As a first step, we can model such a localised control as a linear local velocity-force feedback as in equation (4.10). In particular, following several similar works described in the literature (see for instance Camarri (2015) for a review), we can model the presence of the small wire as a local pure drag force proportional to the local velocity field. This leads it a tensor field $\boldsymbol{C}_1$ in equation (4.9) which is diagonal and equal to $\boldsymbol{C}_1 = -c\,\boldsymbol{I}$, where c is a proportionality constant connecting the local velocity with the drag and $\boldsymbol{I}$ is the identity tensor. If we substitute this particular control tensor in equation (4.10) we obtain the following result quantifying the action of such a control on the Floquet exponent:

$$\delta\sigma = -c\,\mathrm{Tr}\,(\boldsymbol{S}_{tot}) = -c\,(\mathrm{Tr}\,(\boldsymbol{S}_b) + \mathrm{Tr}\,(\boldsymbol{S}_l)) \tag{6.2}$$

As highlighted in equation (6.2), the control is proportional by means of $-c$ to the trace of the sensitivity tensors $\boldsymbol{S}_b$ and $\boldsymbol{S}_l$, and their sum, which corresponds to $\mathrm{Tr}\,(\boldsymbol{S}_{tot})$, provides a control map indicating the quantitative action of the local placement of a control wire on the Floquet exponent. In order to analyse the contributions to the control map deriving from the base flow modifications and from the direct action of the control on the linearised dynamics of the three-dimensional disturbances, we plot both scalar fields $\mathrm{Tr}\,(\boldsymbol{S}_b)$ and $\mathrm{Tr}\,(\boldsymbol{S}_l)$ for mode A in figure 4. Confirming what already observed in section 6.1, the two contributions are equally important for the quantitative evaluation of the effect of control. The total control map, which is the sum of the two maps reported in figure 4, is reported in figure 6(a). Note that the resulting control map is real-valued because the instability mode A is synchronous, so that the vortex shedding frequency remains unchanged when the control is applied. The value in the map express the quantitative variation of σ, which in this case is a pure growth rate. The applied control can be stabilising or destabilising depending on the sign of $\delta\sigma$. In particular, since $c > 0$ as the small control wire always excerts a drag, the effect of control is destabilising when the control map in figure 6(a) is positive valued and destibilising when negatively valued. Thus, inspecting figure 6(a) for instance a control wire positioned in the point $(1.05, 0.0)$ (as done in Zhang *et al.* (1995) as will be commented in a dedicated section) is stabilising for mode A while a wire in $(1.68, 0.0)$ is strongly destabilising.

Analogous comments can be done for the control of mode B. To this purpose we report in figure 5 the $\mathrm{Tr}\,(\boldsymbol{S}_b)$ (a) and $\mathrm{Tr}\,(\boldsymbol{S}_l)$ (b) scalar fields. In this case, as already highlighted

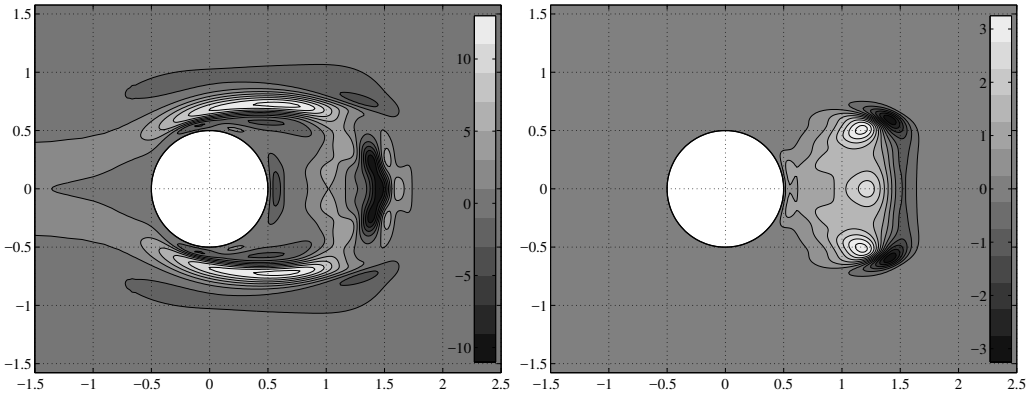

FIGURE 5. Mode B ($Re = 260$, $k = 7.640$): scalar fields (a) $\mathrm{Tr}\,(S_b)$ and b) $\mathrm{Tr}\,(S_l)$.)

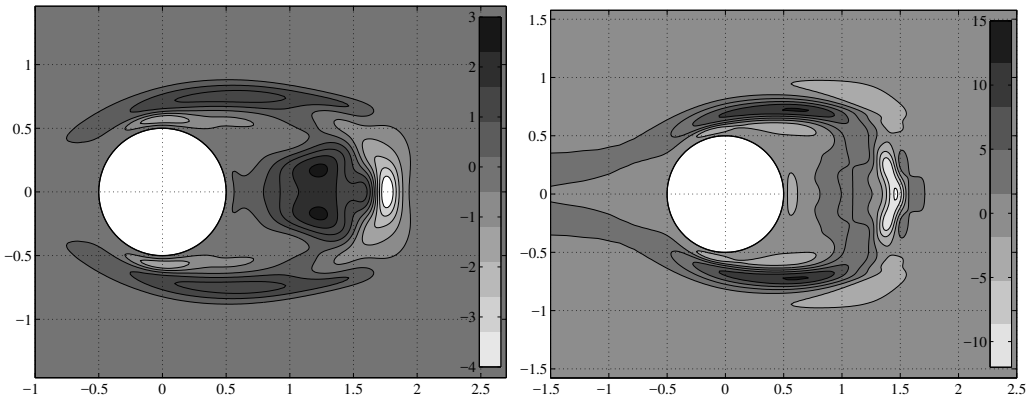

FIGURE 6. Total control map $\mathrm{Tr}\,(S_{tot})$: a) mode A ($Re = 190$, $k = 1.585$) and b) mode B ($Re = 260$, $k = 7.640$).

by the sensitivity analysis, the contribution of the control to the variation of $\delta\sigma$ induced by a variation of the base flow can be one order of magnitude larger than that obtained by the direct action on the linearised dynamics. However, this second contribution (derived from S_l), is important since it is localised in a region where it is of the same order of magnitude of the contribution coming from S_b. The total control map obtained by the sum of the two contributions is plotted in figure 6(b). As for mode A, mode B is synchronous and it remains synchronous in the controlled case, so that $\delta\sigma$ is real-valued. If we compare the total control maps for mode A and B, i.e. figure 6(a) and figure 6(b), is it possible to note that mode B is definitely more sensitive to control. Note however that the two maps are pictures taken at two different values of Re, Lastly, while control for mode A is equally effective if applied in the shear layers and in the wake, mode B is definitely more sensitive to control if this is applied in the shear layers detaching from the body.

Finally, as shown in section 4, a necessary step for the estimation of $\delta\sigma$ is the evaluation of the effect of control on the vortex shedding frequency which is implicitly taken into account in equation 4.10. This point, which is a side output of the analysis, is however very important for control purposes since it provides synthetic control maps as those reported in figure 6 illustrating the effect of a control wire on the non-linearly saturated vortex shedding frequency. In particular, if we model the control wire as proposed above

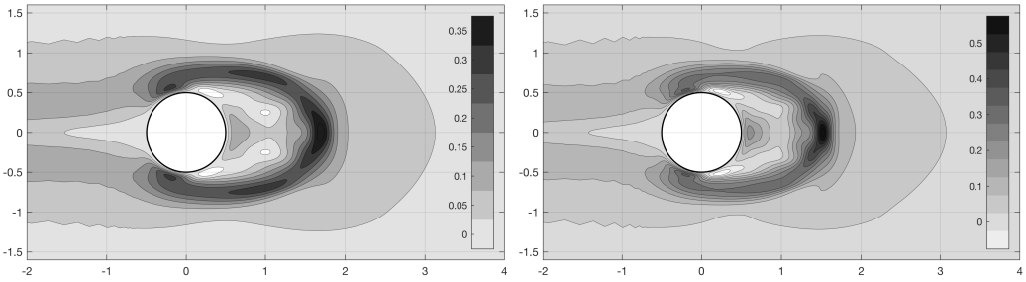

FIGURE 7. Spatial distribution of the scalar field $2\pi\,\mathrm{Tr}\,(\mathsf{S}_s)$: a) mode A ($Re = 190$, $k = 1.585$) and b) mode B ($Re = 260$, $k = 7.64$).

and we substitute the model in equation (4.2) we obtain:

$$\delta S_t = -c\, I : \mathsf{S}_s(x_0, y_0) = -c\,\mathrm{Tr}\,(\mathsf{S}_s)\,(x_0, y_0) \tag{6.3}$$

In this case the only contribution to the variation of the vortex shedding is obviously due to the action of the control on the base flow, as indeed vortex shedding is a property of the base flow. The resulting control map, the scalar field $\mathrm{Tr}\,(\mathsf{S}_s)$, is plotted in figure 7 for mode A (a) and B (b). Note that, even if it is not immediately clear by the figure, the map comprises also negative values in very localised regions just downstream of the separation points of the shear layers. However, except for these vey limited regions the map is positive valued, implying a decrease of the vortex shedding frequency or, equivalently, an increase of its period. Moreover, the effect of the control on δSt is qualitatively and quantitatively similar for modes A and B, that for mode B being larger by only a factor which is roughly equal to 1.6 and not by an order of magnitude as for $\delta\sigma$. In particular, the regions where control mostly affects the vortex shedding frequency is in the boundaries of the mean recirculation region of the wake. For instance, if we constrain the control wire to be on the symmetry line $y = 0$, the position of maximum effect of control for mode A is at $x = 1.69$ ($\delta St = 6.43 \cdot 10^{-2}\, c$) and, for mode B, at $x = 1.51$ ($\delta St = 9.44 \cdot 10^{-2}\, c$).

6.3. *Validation of the control maps by DNS*

In this section we provide a validation of the control maps reported and discussed at section 6.2. The validation has been carried out for both mode A and mode B. Here, for sake of brevity, we just report results concerning mode A.

We have used the code Nek5000 and three-dimensional simulations whose numerical details are provided in section 5. In order to properly discretize a localised drag force without the need of ad-hoc mesh refinements, which might be difficult with a structured grid, and considering that we are using a spectral element method which may be inaccurate if the forcing applied to the equations is not sufficiently regular, we have chosen to replace the Dirac delta in equation (4.9) by a more regular but still quite localised function δ_N in the $x - y$ planes. In particular, the drag force applied to the momentum equations in the DNS is the following:

$$\delta \mathsf{H}_N(x, y, z) = -c_N \underbrace{\left[\frac{1}{\pi\gamma^2}\exp^{-\left(\frac{(x-x_0)^2+(y-y_0)^2}{\gamma^2}\right)}\right]}_{\delta_N(\mathbf{x}-\mathbf{x_0})} \mathbf{U}(x, y, z) \tag{6.4}$$

where c_N is the free proportionality constant of the control and γ is a free parameter determining the sharpness of the resulting function δ_N. Note that the function δ_N is normalised such that i.e. $\int_{-\infty}^{\infty}\int_{-\infty}^{\infty}\delta_N(x, y, x_0, y_0)\mathrm{d}x\,\mathrm{d}y = 1$. In the simulations docu-

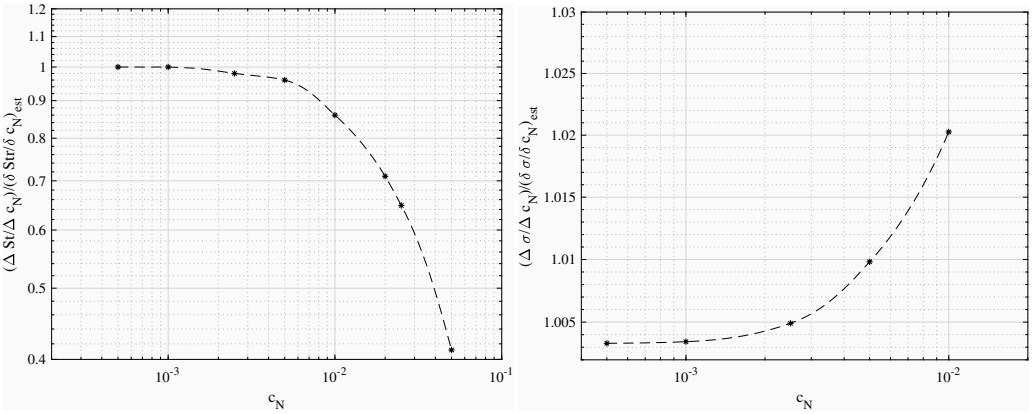

FIGURE 8. Mode A ($Re = 190$, $k = 1.585$): (a) ratio $\frac{(St_c - St_n)/c_N}{\delta St/c_N}$ where St_c and St_n are the Strouhal numbers of vortex shedding obtained by DNS using an intensity control equal to c_N and $\delta St/c_N$ is the value estimated by equation (6.6); (b) ratio $\frac{(\sigma_c - \sigma_n)/c_N}{\delta\sigma/c_N}$ where σ_c and σ_n are the Floquet exponents obtained by DNS using an intensity control equal to c_N and $\delta\sigma/c_N$ is the value estimated by equation (6.5).

mented here we have fixed $\gamma = 0.3$ after having verified that the resulting function δH_N is represented very well by the numerical discretisation used in the DNS, at least for the considered points (x_0, y_0) listed in the following. In particular, the numerical integral of δ_N carried out using the same spectral basis used for the DNS differs from 1 by a quantity of the order of 10^{-6}.

When the forcing in equation (6.4) is substituted in the general equations (4.4) and (4.7), introducing also the sensitivity tensors defined in section 4, we finally obtain the following result for $\delta\sigma$:

$$\delta\sigma = -c_N \int_D \delta_N(x - x_0, y - y_0)\,[\mathsf{S}_b(x, y) + \mathsf{S}_I(x, y)]\,\mathrm{d}\mathcal{D} \tag{6.5}$$

where the forcing is centered around a selected point (x_0, y_0). A similar result is obtained from equation (4.2) for the variation induced on the Strouhal number:

$$\delta St = -c_N \int_D \delta_N(x - x_0, y - y_0)\mathsf{S}_s(x, y)\mathrm{d}\mathcal{D} \tag{6.6}$$

In the validation proposed here we have selected a few points which are of interest for the control. For each of them we have computed the estimated values of $\delta St/c_N$ and $\delta\sigma/c_N$ provided by equations (6.6) and (6.5) and we have compared estimations with the true values of the same quantities, computed by DNS. The value of c_N in the DNS simulations is progressively decreased in order to check convergence towards the theoretically estimated values.

On the basis of the experiments in Zhang *et al.* (1995), one point of interest for the control is point P2, with coordinates $(x_0, y_0) = (1.05, 0.0)$. The results of the validation test described above, which implies a set of DNS simulations, are reported in figure 8(a) and (b) for the Strouhal number and the Floquet exponent of mode A, respectively. In particular, in figure 8(a) we plot the ratio between the quantity $(St_c - St_n)/c_N$, where St_c and St_n are the Strouhal numbers of vortex shedding in the controlled and uncontrolled case respectively, computed by DNS using c_N, and the value $\delta St/c_N$ estimated by equation (6.6). The ratio must tend approximately to 1 when the value c_N is progressively decreased if the provided maps are correct. The limit can be slightly different

Point	Tr (S_b)	Tr (S_I)	Tr $(S_t) = \delta\sigma/c_N$	Tr $(S_s) = \delta St/c_N$
P1	0.323	0.123	0.446	0.140
P2	0.550	1.019	1.569	0.050
P3	-0.995	0.627	-0.368	0.214

TABLE 1. Mode A ($Re = 190$, $k = 1.585$): effect of the control in equation (6.4) on $\delta\sigma$, separating the two contributions coming from S_b and S_I, and on δSt, for three different points of application of the control.

than 1 since the validation by DNS is carried out with a numerics which is completely different from that used in deriving the control maps. Figure 8(a), where we report the resulting convergence curves, clearly show convergence of the results. Moreover, the final number obtained for the lowest value of C_N ($C_N = 5 \cdot 10^{-3}$) is equal to 1 to the accuracy of the calculations, indicating a perfect convergence which validates not only the related control map but also the implementation of the solvers and the numerical resolution used both for the maps and for DNS.

In figure 8(a) we carry out the same analysis but focusing on the ratio between $(\sigma_c - \sigma_n)/c_N$, where σ_c and σ_n are the Floquet exponents of mode A in the controlled and uncontrolled case, respectively, computed by DNS using c_N, and the value $\delta\sigma/c_N$ estimated by equation (6.5). In this case the final error between the estimated and the computed value of $\delta\sigma/c_N$ is of the order of 0.3%. This is plausible since the estimation of σ by DNS is delicate and in general more difficult than that of the Strouhal number. The same validation has been carried out for other two points, P1 $(0.75, 0.75)$ and P3 $(0., 1.68)$, with results analogous to those for P2 and not reported here for the sake of brevity. We report however the corresponding control estimations, together with that for point P2, in table 1 where we split the contributions related to the two sensitivity tensors, S_b and S_I so as to highlight the relative contributions coming from the modification of the baseflow and from the direct action of the control on the perturbation dynamics to the final result. As already pointed out, the two contributions for mode A are of the same order of magnitude, and thus both of them must be taken into account for a proper estimation of the effects of control on the instability. Moreover, table 1 also shows that while the control is stabilising when positioned on points P1 and P2, it is destabilising on P3. In particular point P3 is interesting because the effect on $\delta\sigma$ coming from S_b and S_I are opposite, i.e. the first is destabilising and the second is stabilising. In the sum of the two, the destabilising contribution is dominant. This is an example in which a control map solely based on S_I is not only quantitatively but also qualitatively wrong. As concerns the Strouhal number, controls applied on all points P1, P2 and P3 all lead to a decrease of the vortex shedding frequency. As an overall qualitative and comparative inspection of the effect of the mentioned controls, they have been applied to the flow at $Re = 220$ starting from the same initial conditions, in which mode A is at the very first stage of development. A slightly larger value of Re instead of $Re = 190$ has been chosen in order to better show the behaviour of the different controls by DNS. The resulting z-component of the velocity on a point in the wake (coordinates $(0.6, 0.8, 0)$) are reported together with the uncontrolled case (dashed line) in figure 9. Inspecting figure 9 and zoomed view reported in figure 9(b), it is possible to verify by visual inspection that control on P3 is destabilising, while on P1 and P2 is stabilising. Moreover, as predicted by the maps control on P2 is more stabilising than that on P1. Finally, in all cases the period of vortex shedding increases with respect to the uncontrolled one, the effect being less important when control is applied on P2.

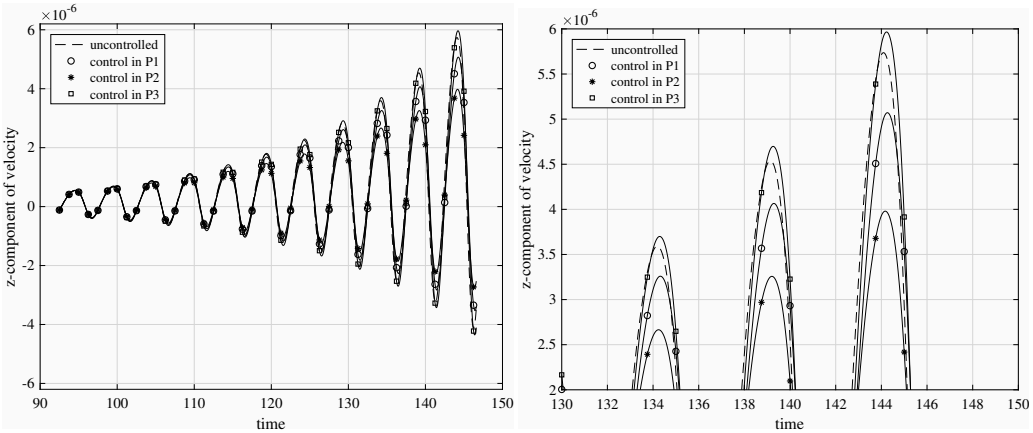

FIGURE 9. Mode A ($Re = 220$, $k = 1.585$), DNS: instantaneous z-component of the velocity field on the point $(0.6, 0.8, 0)$ showing the very stage development of mode A in the uncontrolled case (dashed line) and in the controlled case when control in equation (6.4) is applied to points P1, P2 and P3; subfigure (b) is a zoomed view of subfigure (a).

6.4. *Estimating experimental results in Zhang et al. (1995) by control maps*

In this section we will try to provide a rough quantitative estimation of the results obtained in Zhang *et al.* (1995) as concerns the secondary instability in the wake past a circular cylinder when this is controlled by a small wire. They observed that the wire could suppress the instability leading to a two dimensional flow. This was observed for instance for $Re = 219$ when the wire, whose diameter was $d = 25\,\mu m$ was placed on point P2 $(1.05, 0)$. In that set of experiments the diameter of the main cylinder was $D = 4\,\text{mm}$, leading to $d/D = 6.3 \cdot 10^{-3}$. It was also observed that at $Re = 230$ the instability started again. This behavior can be predicted, as it will be shown here, using the control maps reported in section 6.2. To this purpose, as a first step we have extracted the velocity field simulated at $Re = 220$ in the two dimensional case, observing that the maximum velocity was equal to $0.79\,U_\infty$, this leading to a maximum Reynolds number based on d and on the local velocity equal to $Re_{d,max} \simeq 1.08$. We assume a quasi-static behavior of the drag excerted by the flow on the control wire, with the drag coefficient normalised with the diameter d of the wire and the local velocity given by the Lamb's law (see for instance Landau & Lifshitz (1987)):

$$C_{d,wire}(Re_d) = \frac{8\pi}{Re_d}\,(2.0024 - \log(Re_d)) \tag{6.7}$$

The cartesian components of the resulting force in one shedding period computed using the local velocity and the Lamb law in equation (6.7) and normalised using U_∞ and D are reported in figure 10 with a continuous line. The force is approximated by a linear force-velocity feedback and the coefficient of proportionality c is tuned so as to fit the true forces reported in figure 10 in a least-square sense. The resulting value, $c \simeq 2.68 \cdot 10^{-2}$, leads to the estimated force components plotted in dashed line in figure 10. By the comparison between the true (continuous) and the approximate force (dashed) lines it is possible to see that the fit provided by the tuned linear model can be considered satisfactory. Once the constant c has been estimated, by mutiplying its value with the value assumed by the control map on the point P2 (see figure 6(a)) we obtain the estimated variation of the Floquet exponent, which in this case is equal to $\delta\sigma = -0.057$. The value of the Floquet exponent at $Re = 220$ has been computed by DNS and it is equal to $\sigma_{220} = 0.047$. Since

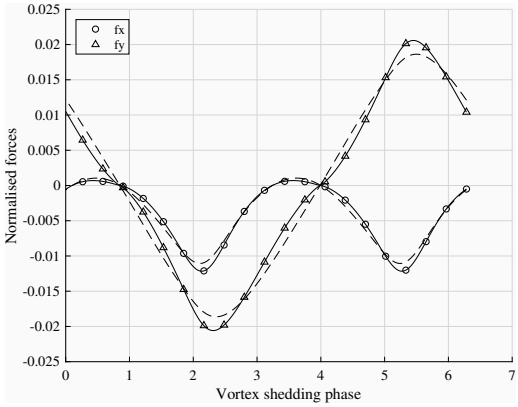

FIGURE 10. Cartesian components of the force acting on the control wire at $Re = 220$: quasi-static model based on Lamb's equation in continuous lines and tuned linear model in dashed lines.

the modified Floquet exponent is negative, i.e. $\sigma_{220} + \delta\sigma < 0$, the control map predicts a stabilisation of the flow field, in agreement with the experiments in Zhang *et al.* (1995). At $Re = 230$ the floquet exponent is equal to $\sigma_{230} = 0.0625$. In this case, since $\delta\sigma$ remains approximately the same, we have $\sigma_{230} + \delta\sigma > 0$, i.e. the control wire is not sufficient to stabilise the flow, again in agreement with the experiments. In the calculations detailed above we have assumed for simplification that the control map for mode A at $Re = 220$ is not significantly different from that at $Re = 190$ reported in figure 6(a). However, we have verified by DNS that variations of $\delta\sigma/c$ on point P2 for mode A are of the order of 15% between $Re = 190$ and $Re = 220$, which makes our approximation acceptable.

The procedure illustrated above has been repeated for another point, P1 (already defined in section 6.3, the coordinates being $(0.75, 0.75)$), since in the experiments by Zhang *et al.* (1995) mode A is stabilised for that wire position when $Re < 270$. Extrapolating again the control maps computed at $Re = 190$, we estimate that a wire of the same size as that used in the experiments leads to $\delta\sigma = -0.0845$ in the controlled case. Since $\sigma_{230} = 0.0625$ we can deduce that the flow is stabilised, according to our theoretical estimation. Moreover, considering that the Floquet exponent for $Re = 260$ is approximately equal to $\sigma_{260} = 0.0910$ we can deduce by linear interpolation of the Floquet exponent between $Re = 230$ and $Re = 260$ that the wire in position P1 leads to a stabilisation of mode A up to $Re \simeq 254$, which is in fairly good agreement with Zhang *et al.* (1995) where it seems that stabilisation is active up to $Re = 260$.

7. Conclusions

In this paper we have presented a general theoretical methodology for conducting sensitivity analysis with respect to a generic forcing acting on the baseflow for cases in which the baseflow is periodic in time. At difference with the analysis considered previously by Giannetti *et al.* (2010), where the effects of a perturbation acting solely on the disturbance equations is investigated, we now study the sensitivity of the Floquet exponent when a structural perturbation is acting on the base flow equations. The effects of such a perturbation is able to generate a change of the base flow which, in turn, affects the stability equations through a change of the coefficients of the Linearised Navier-Stokes operator. Here we derive the expression of the sensitivity tensor for the Floquet exponent of a given instability and for the frequency of the saturated limit cycle of the base flow

with respect to a generic forcing of the base flow itself. In this respect the present work and that in Giannetti *et al.* (2010) can be considered an extension of the seminal work by Marquet *et al.* (2008) and Luchini *et al.* (2009) to the case of base flows which are periodic in time.

Although the theory proposed here is general, it has been specialised since the beginning so as to study the second bifurcation of the flow past a circular cylinder. Sensitivity results for two nearly marginally stable flow conditions are discussed: Reynolds number $Re = 190$ is selected to study mode A while $Re = 260$ is adopted to investigate mode B.

Firstly we started to discuss the differences between the spectral norm of the structural sensitivity tensors computed in Giannetti *et al.* (2010) and the sensitivity tensors representing the sensitivity to a base flow variation derived here. Both the resulting spatial maps are highly localised in the flow region immediately past the bluff body. We note that the sensitivity to base flow forcing for mode A is similar to the one of mode B. However, the sensitivity of the mode B is characterised by higher values with respect to the other sensitivity maps.

The analysis presented here is successively used to build up control maps for the passive control that might be obtained by placing a small wire in the flow. Besides being interesting by itself for control purposes, this kind of control has been already applied in the literature by Zhang *et al.* (1995), so that results from that paper can be used to assess the accuracy of the predictions provided by the theory proposed here. For this kind of control, assuming that the control wire experiences a pure drag force, we can build control maps predicting the variation of the Strouhal number of the vortex shedding and of the Floquet exponent for a given instability mode (A or B) vs a generic position of the wire. The resulting maps have been discussed and validated using DNS. Validation proved that they are correct and accurate. Lastly, the information provided by the derived control maps have been used in a dedicated section so as to predict the control experiments documented in Zhang *et al.* (1995) demonstrating that quantitative agreement between experiments and theory is definitely satisfactory.

Summarising, the main outputs of the present work are mainly two. On one side we propose a general theory for the design of passive controls of instabilities developing on time-periodic base flows. On the other side, by applying this methodology, we provide original results on a classical but still actively studied problem in the literature, which is the secondary instability of the wake past a circular cylinder.

REFERENCES

Barkley, D. & Henderson, R. D. 1996 Three-dimensional floquet stability analysis of the wake of a circular cylinder. *J. Fluid Mech.* **322**, 215–241.

Bottaro, A., Corbett, P. & Luchini, P. 2003 The effect of base flow variation on flow stability. *J. Fluid Mech.* **476**, 293–302.

Brandt, L., Sipp, D., Pralits, J. O. & Marquet, O. 2011 Effect of base-flow variation in noise amplifiers: the flat-plate boundary layer. *J. Fluid Mech.* **687**, 503–528.

Camarri, S. 2015 Flow control design inspired by linear stability analysis. *Acta Mechanica* **226** (4), 979–1010.

Camarri, S., Fallenius, B. & Fransson, J. 2013 Stability analysis of experimental flow fields behind a porous cylinder for the investigation of the large-scale wake vortices. *J. Fluid Mech.* **715**, 499–536.

Davis, T. A. 2004 Algorithm 832: Umfpack, an unsymmetric-pattern multifrontal method. *ACM Transactions on Mathematical Software* **30** (2), 196–199.

Drazin, P. G. 2002 *Introduction to Hydrodynamic Stability*. Cambridge University Press.

Gavarini, I., Bottaro, A. & Nieuwstadt, F. T. M. 2004 The initial stage of transition in pipe flow: role of optimal base-flow distortions. *J. Fluid Mech.* **517**, 131–165.

Giannetti, F., Camarri, S. & Luchini, P. 2010 Structural sensitivity of the secondary instability in the wake of a circular cylinder. *J. Fluid Mech.* **651**, 319–337.

Giannetti, F. & Luchini, P. 2007 Structural sensitivity of the cylinder first instability of the cylinder wake. *J. Fluid Mech.* **581**, 167–197.

Landau, L. D. & Lifshitz, E. M. 1987 *Fluid Mechanics, Second Edition: Volume 6 (Course of Theoretical Physics)*. Butterworth-Heinemann.

Luchini, P. & Bottaro, A. 2014 Adjoint equations in stability analysis. *Annu. Rev. Fluid Mech.* **46**, 493–517.

Luchini, P., Giannetti, F. & Pralits, J. 2009 Structural sensitivity of the finite-amplitude vortex shedding behind a circular cylinder. *IUTAM Symposium on Unsteady Separated Flows and their Control* pp. 151–160.

Marquet, O., Sipp, D. & Jacquin, L. 2008 Sensitivity analysis and passive control of cylinder flow. *J. Fluid Mech.* **615**, 221–252.

Noack, B. R., König, M. & Eckelmann, H. 1993 Three-dimensional stability analysis of the periodic flow around a circular cylinder. *Phys. Fluids* **A 5 (6)**, 1279–1281.

Noak, B. R. & Eckelmann, H. 1994 A global stability analysis of the steady and periodic cylinder wake. *J. Fluid Mech.* **270**, 297–330.

Rai, M. M. & Moin, P. 1991 Direct simulations of turbulent flow using finite-difference schemes. *J. Comp. Phys.* **96**, 15–53.

Sipp, D., Marquet, O., Meliga, P. & Barbagallo, A. 2010 Dynamics and Control of Global Instabilities in Open-Flows: A Linearized Approach. *Appl. Mech. Rev.* **63** (3), 030801.

Williamson, C. H. K. 1988 The existence of two stages in the transition to three-dimensionality of a cylinder wake. *Phys. Fluids* **31**, 3165–3168.

Zhang, H. Q., Fey, U. F. & Noack, B. R. 1995 On the transition of the cylinder wake. *Phys. Fluids* **7 (4)**, 779–794.